Supplement of Atmos. Chem. Phys., 25, 13687–13710, 2025 https://doi.org/10.5194/acp-25-13687-2025-supplement © Author(s) 2025. CC BY 4.0 License.





## Supplement of

## **Urban Area Observing System (UAOS) simulation experiment using DQ-1 total column concentration observations**

Jinchun Yi et al.

Correspondence to: Ge Han (udhan@whu.edu.cn)

The copyright of individual parts of the supplement might differ from the article licence.

Table S1 Several primary parameters of ACDL(Fan et al., 2024)

Parameters	Values		
Oribit altitude	705km		
Lidar footprint diameter	~70m		
Horizontal spacing of lidar footprints	~350m		
Field of view	<0.2mrad		
Telescope diameter	1000nm		
Divergence angle after laser beam expansion	<0.1mrad		
Repetition frequency	20Hz		
Laser pulse width	<50ns		
Laser energy	75mJ		
Off-line wavelength	1572.085nm		
On-line wavelength	1572.024nm		

Table S2 Model version information used in this study.

Model	Version
STILT(Stochastic Time-Inverted Lagrangian Transport)	V2
WRF(Weather Research and Forecasting)	V4.0
X-STILT(X-Stochastic Time-Inverted Lagrangian Transport	V1
model)(Wu et al., 2018)	

Table S3 Comparison with the OCO-2 Background Method

City	Overpass	Ye et al.'s method(Ye et al.,	DWT method Scaling	The whole city emissions	
		2020) Scaling factor( $\lambda$ ) $\pm$	$factor(\lambda)$ $\pm$ posterior	(Mt C/month)	
		posterior uncertainty ( $\hat{\sigma}$ )	uncertainty ( $\hat{\sigma}$ )		
Riyadh	02 March 2023	$0.75 \pm 0.18$	$0.75 \pm 0.20$	2.3	
	20 June 2022	$0.86 \pm 0.16$	$0.86 \pm 0.16$	3.3	
Beijing	01 December 2022	$0.98 \pm 0.15$	$0.98 \pm 0.15$	3.3	
	08 April 2023	$0.65 \pm 0.11$	$0.65 \pm 0.11$	2.4	
	09 January 2023	$0.91 \pm 0.12$	$0.91 \pm 0.12$	3.5	
	10 January 2023	$1.00 \pm 0.14$	$1.00 \pm 0.14$		
	19 June 2022	$0.96 \pm 0.16$	$0.96 \pm 0.16$	2.9	
	20 June 2022	0.53±0.12	0.53±0.11		
Cairo	26 June 2022	1.06±0.20	1.06±0.20	2.2	
	02 August 2022	0.98±0.12	0.98±0.12	2.4	
	16 August 2022	1.21±0.14	1.21±0.14		
	08 November 2022	1.15±0.15	1.15±0.16	1.9	
	15 November 2022	1.19±0.11	1.19±0.11		
	22 November 2022	1.06±0.13	1.06±0.13		

Note: results derived using the two background estimation methods are highlighted in red when they differ

Table S4 DQ-1 Orbital transit meteorological conditions

City	Overpass	Humidity (%)	Barometer (mbar)	Weather	Temperature ( $^{\circ}$ C)	Vegetation
						Dormant
Riyadh	02 March 2023	24	1019	Passing clouds	29/13	No
	20 June 2022	7	1004	Sunny	46/28	
Beijing	01 December 2022	18	1033	Haze	0/-7	Yes
	08 April 2023	37	1004	Haze	24/8	
	09 January 2023	52	1031	Sunny	7/-6	
	10 January 2023	19	1026	Sunny	7/-6	
	19 June 2022	72	1002	Haze	34/23	
	20 June 2022	52	998	Cloudy	34/23	
Cairo	26 June 2022	27	1010	Sunny	35/23	No
	02 August 2022	40	1005	Passing clouds	35/26	
	16 August 2022	40	1009	Sunny	33/25	
	08 November 2022	68	1014	Clear	25/19	
	15 November 2022	72	1018	Haze	23/17	
	22 November 2022	82	1016	Fog	24/18	

Note: Historical weather data were retrieved from Timeanddate.com, which uses CustomWeather sourced from WMO-certified airport stations and MADIS community stations, with update intervals ranging from 30 min to hourly (https://www.timeanddate.com/weather).

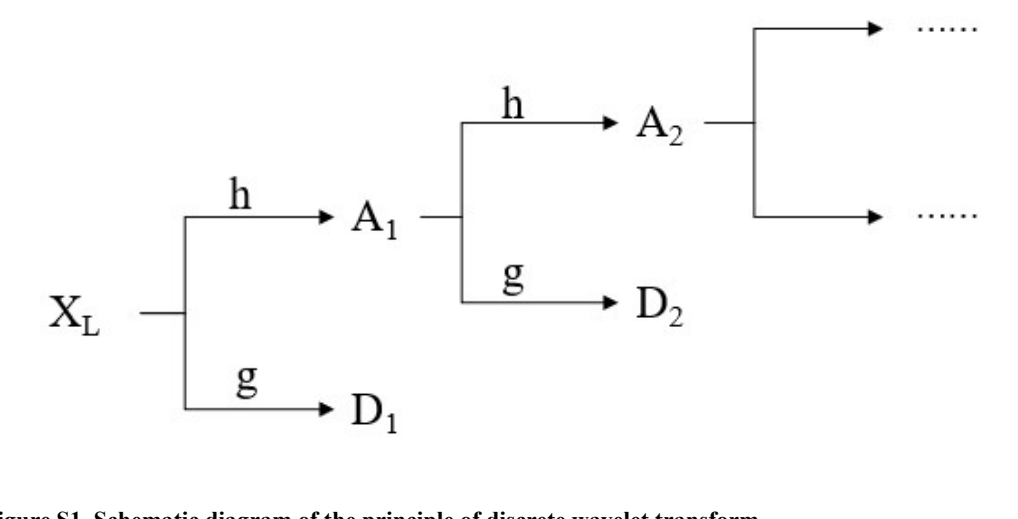


Figure S1. Schematic diagram of the principle of discrete wavelet transform

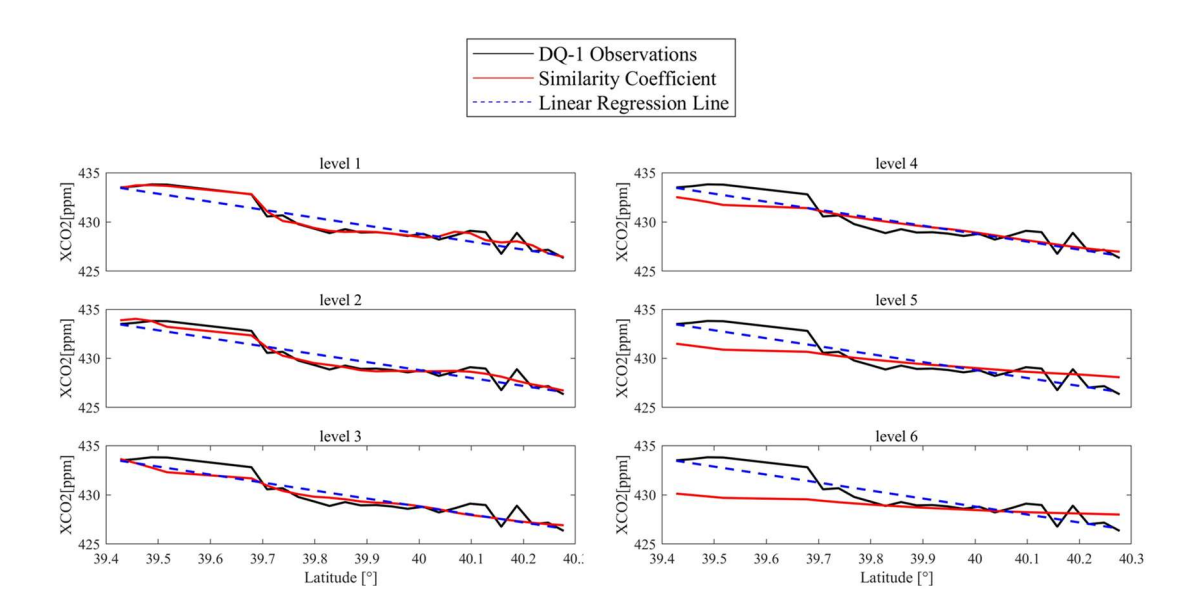


Figure S2. Level 1-6 wavelet transform applied to  $XCO2_{trend}$  (red line in figure) derived from DQ-1 orbital pseudo-data (black line in figure) and  $XCO2_{trend}$  derived from linear regression (blue dashed line in figure) for the DQ-1 orbital pseudo-data (black line in figure) transiting Beijing on 01 December 2022

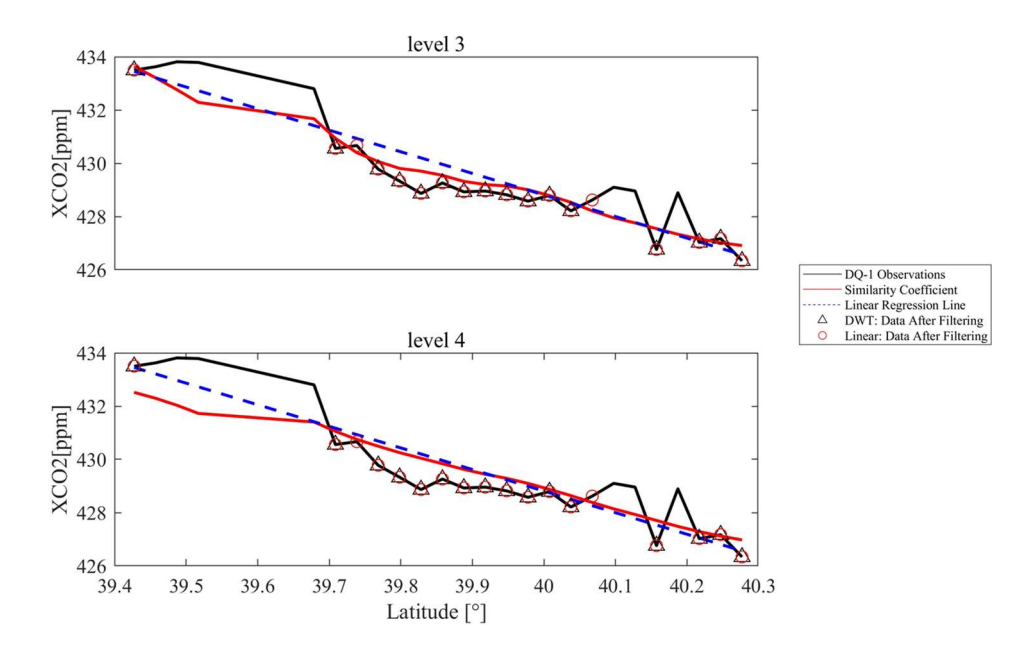


Figure S3. Pseudo-data points involved in the computation of the background line (black hollow triangles in the figure) screened using the third- and fourth-level wavelet transforms, respectively, and background points (red hollow circles) screened using linear regression. The black, red line and blue dashed line are the same as defined in Figure S2.

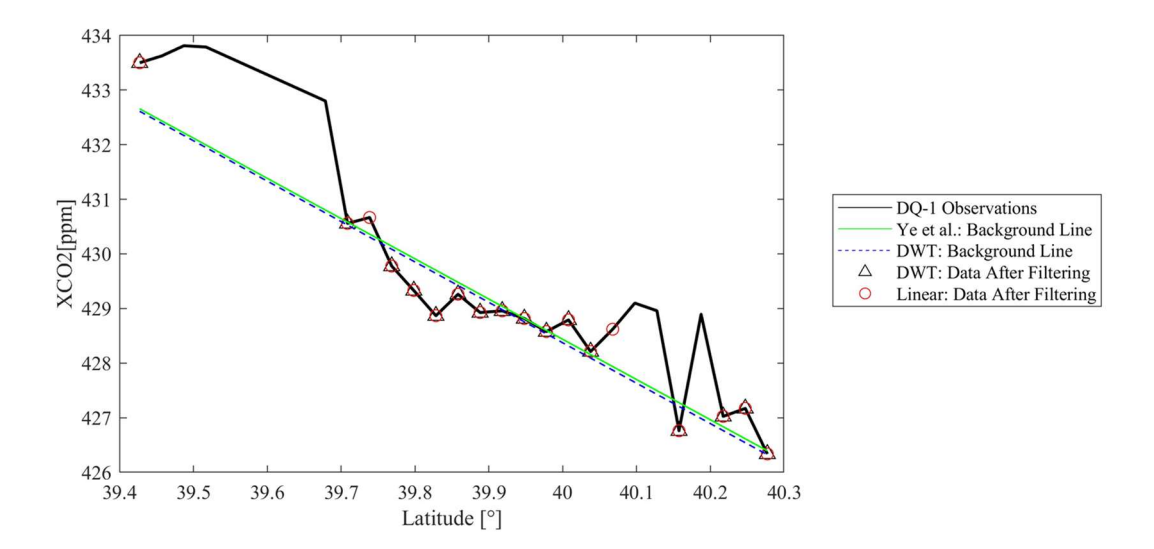


Figure S4. Background line derived using DWT (blue dashed line) and background line derived from linear regression (green line). The black line represents pseudo-observations from DQ-1, the black hollow triangles are background points filtered using DWT, and the red hollow circles are background points filtered by linear regression.

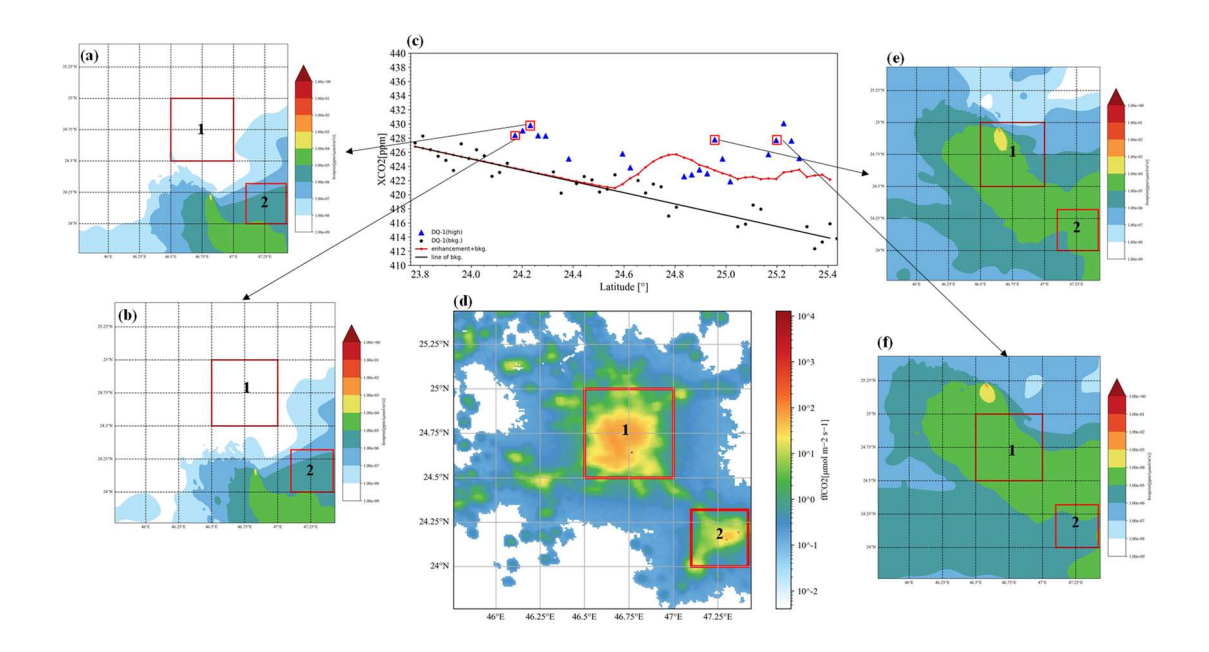


Figure S5. Shows the XSTILT (a, b, e, f) at the location of the partially apparent XCO2 enhancement in the orbit in Fig. 3a of the manuscript. Panel c is Figure 3a from the manuscript and panel d represents the fossil fuel emission inventory now of orbital transit. The main emission sources in the urban area are boxed in red.

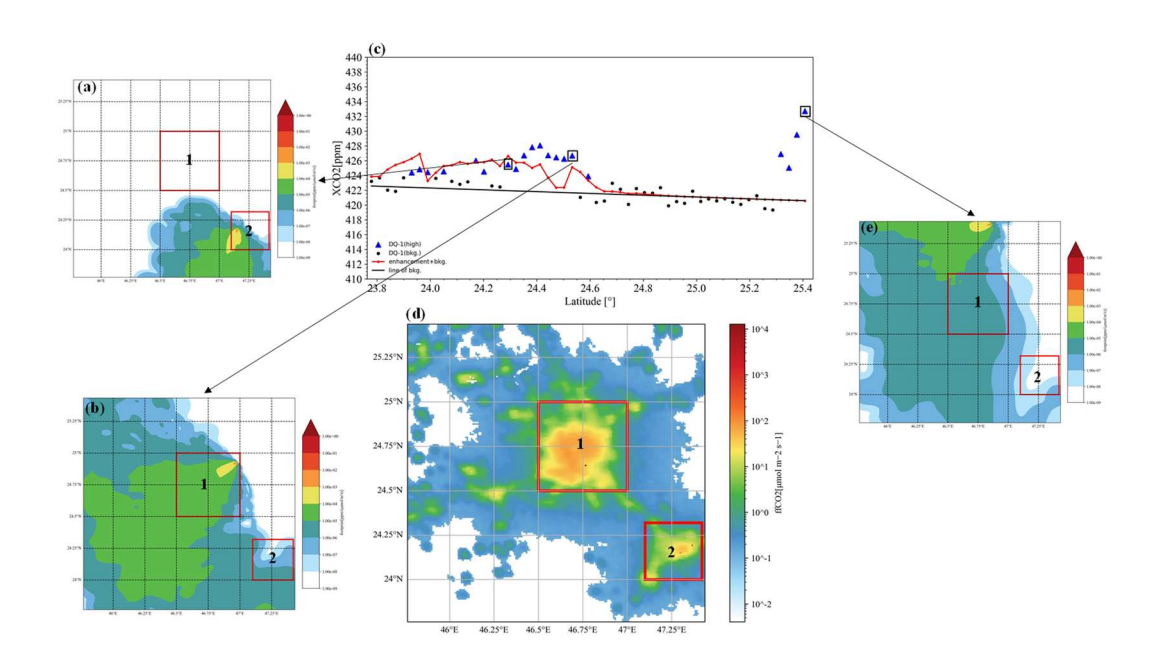


Figure S6. Like Fig. S5, the XSTILT for the case of Fig. 3b in the manuscript is shown (a, b, e).

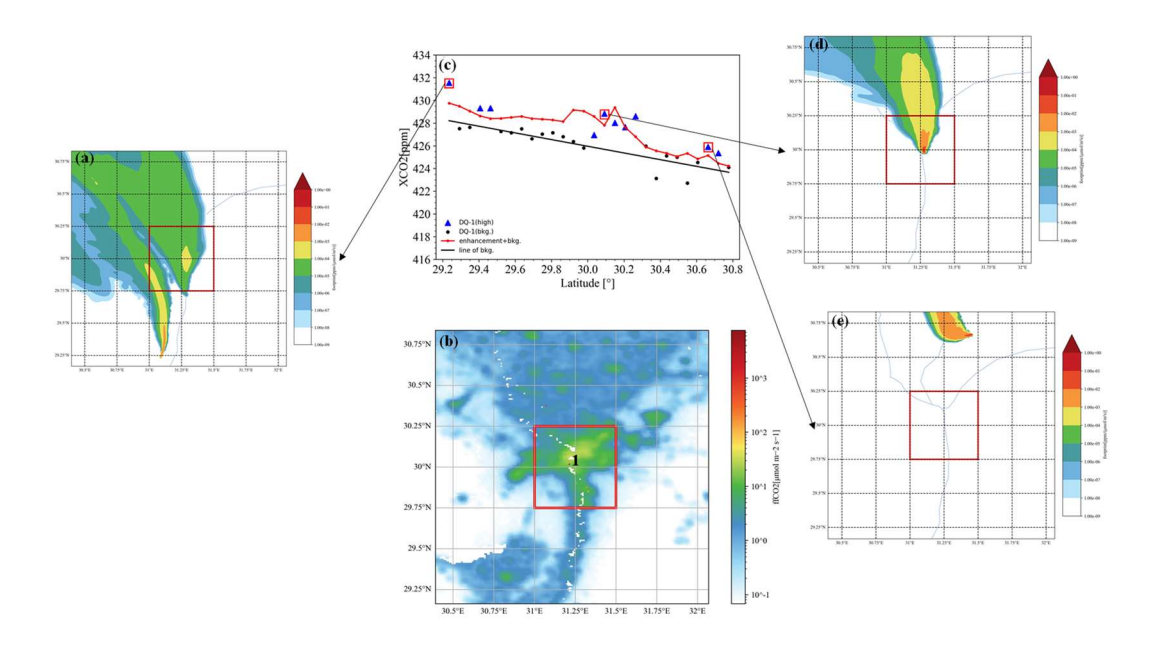


Figure S7. Similar to Figures S5 and S6, XSTILT and enhancement sources are shown for the XCO2 enhancement position of a portion of the DQ-1 orbit transiting Cairo on 15 November 2022 under complex wind conditions

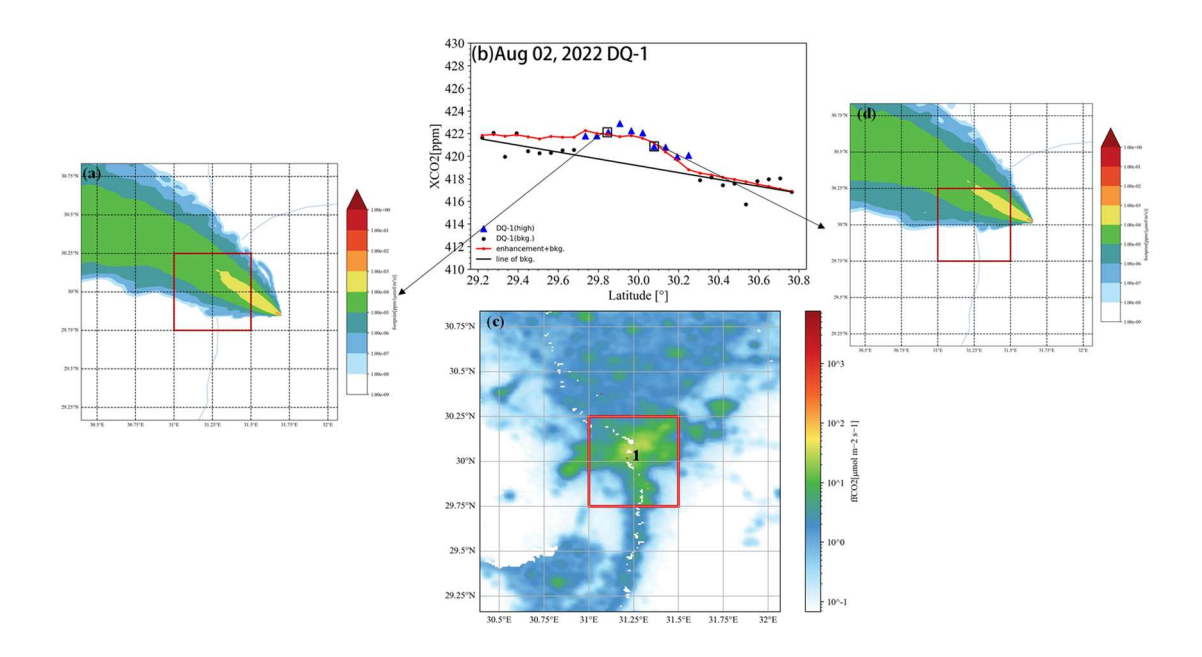


Figure S8. Similar to Figures S5 and S6, XSTILT and enhancement sources are shown for the XCO2 enhancement position of a portion of the DQ-1 orbit transiting Cairo on 02 August 2022 for complex wind conditions

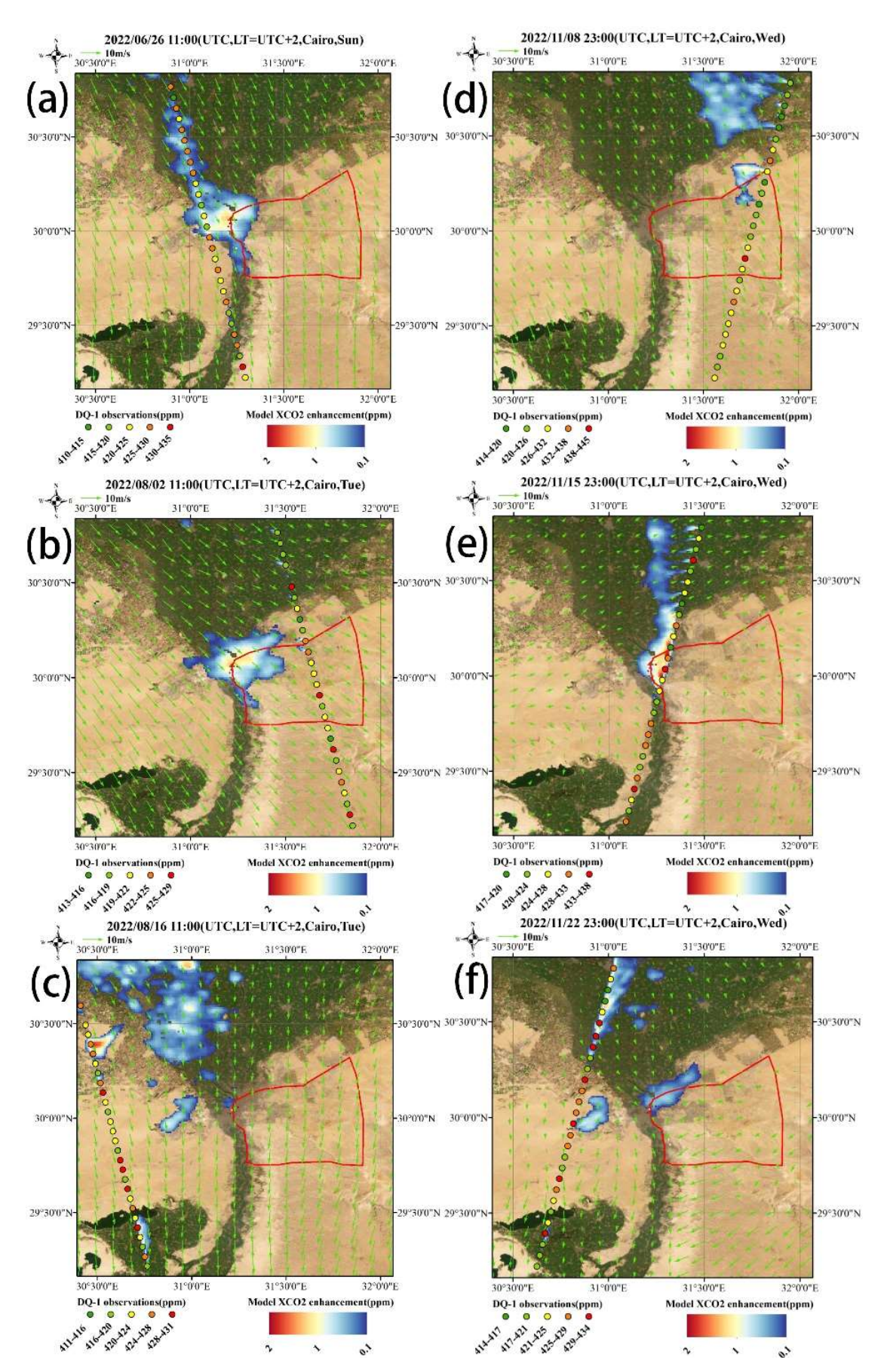


Figure S9. Similar to Fig. 3, but for the trajectories of DQ-1 over Cairo on June 26 (Fig.S9 a), August 02

(Fig.S9 b), August 16 (Fig.S9 c) at 11:00 UTC, November 08 (Fig.S9 d), November 15 (Fig.S9 e), and November 22 (Fig.S9 f) at about 23:00 UTC in 2022. The red boxes in the Figure S9 represent the urban areas.

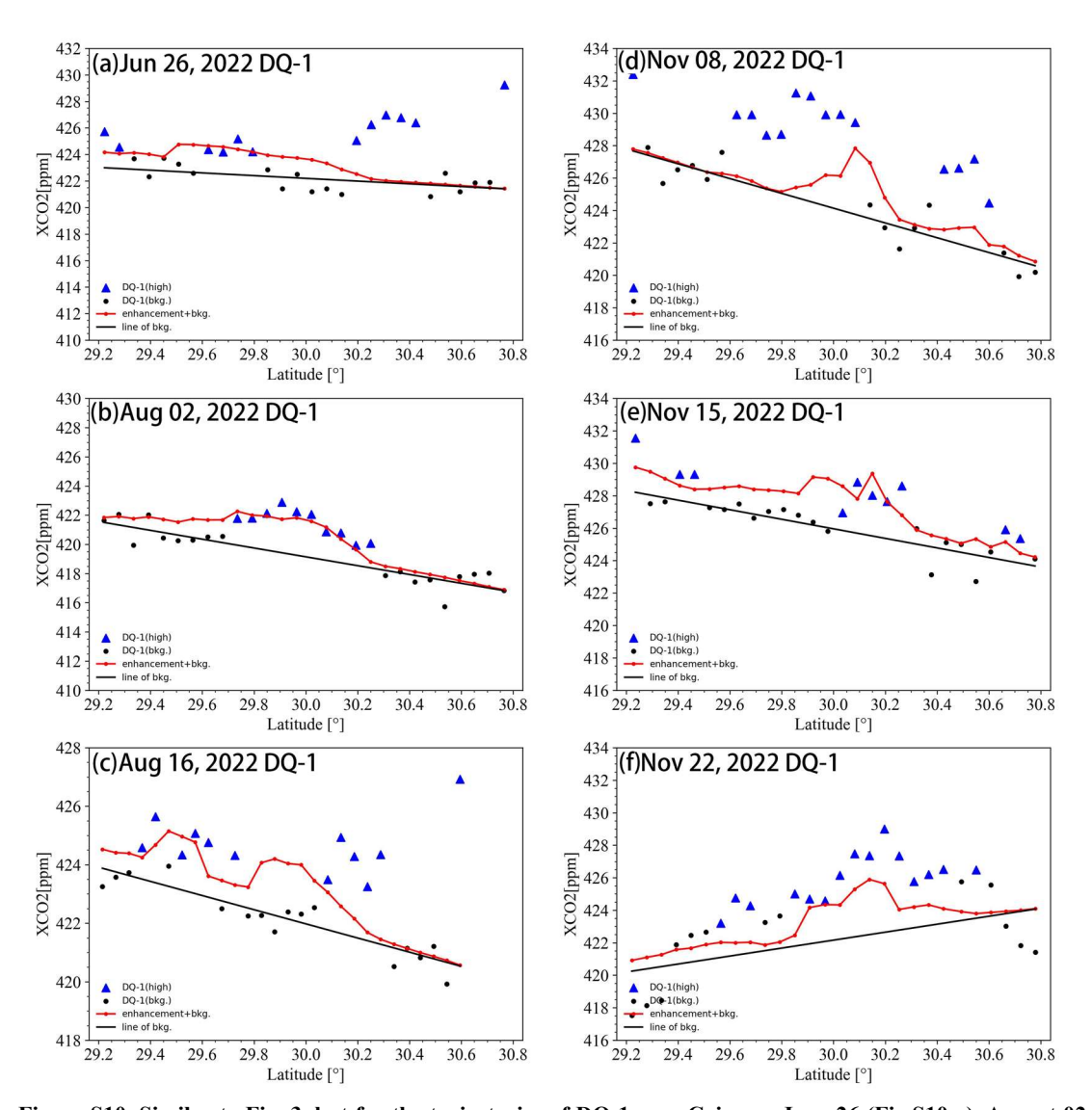


Figure S10. Similar to Fig. 3, but for the trajectories of DQ-1 over Cairo on June 26 (Fig.S10 a), August 02 (Fig.S10 b), August 16 (Fig.S10 c) at 11:00 UTC, November 08 (Fig.S10 d), November 15 (Fig.S10 e), and November 22 (Fig.S10 f) at about 23:00 UTC in 2022.

## References

- Fan, C., Chen, C., Liu, J., Xie, Y., Li, K., Zhu, X., Zhang, L., Cao, X., Han, G., Huang, Y., Gu, Q., and Chen, W.: Preliminary analysis of global column-averaged CO2 concentration data from the spaceborne aerosol and carbon dioxide detection lidar onboard AEMS, Opt. Express, 32, 21870-21886, 10.1364/OE.517736, 2024.
- Wu, D., Lin, J. C., Fasoli, B., Oda, T., Ye, X., Lauvaux, T., Yang, E. G., and Kort, E. A.: A Lagrangian approach towards extracting signals of urban CO2 emissions from satellite observations of atmospheric column CO2 (XCO2): X-Stochastic Time-Inverted Lagrangian Transport model ("X-STILT v1"), Geosci. Model Dev., 11, 4843-4871, 10.5194/gmd-11-4843-2018, 2018.
- Ye, X., Lauvaux, T., Kort, E. A., Oda, T., Feng, S., Lin, J. C., Yang, E. G., and Wu, D.: Constraining Fossil Fuel CO2 Emissions From Urban Area Using OCO-2 Observations of Total Column CO2, Journal of Geophysical Research: Atmospheres, 125, e2019JD030528, <a href="https://doi.org/10.1029/2019JD030528">https://doi.org/10.1029/2019JD030528</a>, 2020.